nature communications

Article

https://doi.org/10.1038/s41467-025-57249-z

Enhanced energy storage performance of nano-submicron structural dielectric films by suppressed ferroelectric phase aggregation

Received: 7 November 2024

Accepted: 17 February 2025

Published online: 26 February 2025

Check for updates

Kun Xing[1,2], Yanan Hao[1], Xin-Jie Wang[2], Lei Huang[2], Yi Gao[1], Tong Liang[1], Yan Meng[1], Ke Bi[1] ✉, Shao-Long Zhong[2] ✉ & Zhi-Min Dang[2] ✉

Maintaining high charge/discharge efficiency while enhancing discharged energy density is crucial for energy storage dielectric films applied in electrostatic capacitors. Here, a nano-submicron structural film comprising ferroelectric material P(VDF-HFP) and linear dielectric material PMMA has been flexibly designed via the electrospinning process. Nano-submicron structure enables the film to maximize the ferroelectric material component and obtain improved dielectric performance without sacrificing breakdown strength and charge/discharge efficiency. As a result, the 40%-420 nm PMMA-P(VDF-HFP) @PMMA sample achieved an discharged energy density of 13.72 J/cm³ at a field of 740 kV/mm, with an impressive charge/discharge efficiency of 80%. This work presents a composite dielectric film that excels in breakdown strength, discharged energy density, and charge/discharge efficiency, offering a strategy for designing reliable, industrial-grade energy storage dielectrics.

Dielectric capacitors, celebrated for their swift charge/discharge capabilities, high power density, and reliable energy storage, are indispensable in a multitude of contemporary electronic and electrical applications, ranging from power systems to pulse systems and renewable energy sources[1–5]. Polymer dielectrics, the materials of choice for dielectric capacitors, are favored for their lightweight nature, ease of processing, robust breakdown strength, and self-healing capabilities[6–8]. However, the limitation of polymer dielectrics is their relatively low discharged energy density, which presents a significant barrier to the miniaturization and integration of electronic devices. At present, state-of-the-art commercial electrostatic capacitors utilize biaxial stretched polypropylene film (BOPP) as the dielectric material, with a dielectric constant of merely 2.2[9], insufficient to satisfy the escalating energy demands of contemporary society[10,11]. This shortfall highlights an urgent need for the evolution of dielectric materials that can offer enhanced energy storage in a compact design. The charged energy density stored in a linear dielectric material can be calculated as $U_e = 1/2\varepsilon_0\varepsilon_r E_b^2$, where ε_0 is the vacuum dielectric constant, and ε_r and E_b are the relative permittivity and breakdown strength of the material, respectively. Therefore, improving the charged energy density requires increasing the ε_r and E_b as much as possible. Furthermore, the often-overlooked charge/discharge efficiency that is defined as the ratio of discharged energy density to charged energy density ($\eta = U_d/U_e$, where U_d is the discharged energy density, and U_e is the charged energy density) is crucial for dielectric capacitor applications. Inadequate efficiency can result in energy waste and Joule heat, exacerbating performance degradation and safety concerns[12–14]. Thus, improving the dielectric's discharged energy density must go hand in hand with maintaining high charge/discharge efficiency[15]. Progressing in this area is essential to meet the escalating energy demands and to align with the rapidly advancing technological landscape across various industries.

Current research is centered on embedding high permittivity (high-K) ceramic fillers within polymer matrices to enhance the capacitive characteristics of polymers[16–22]. Both experimental and simulation data demonstrate that a substantial loading of these fillers can significantly increase the dielectric constant of the composites[16]. However, with the incorporation of a high volume of ceramic particles,

[1]State Key Laboratory of Information Photonics and Optical Communications, School of Science, Beijing University of Posts and Telecommunications, Beijing, China. [2]State Key Laboratory of Power System Operation and Control, Department of Electrical Engineering, Tsinghua University, Beijing, China. ✉e-mail: bike@bupt.edu.cn; slzhong@mail.tsinghua.edu.cn; dangzm@tsinghua.edu.cn

the huge difference in dielectric constant between the ceramic particles and the polymer matrix will lead to severe local electric field concentration within the material, followed by a sharp drop in breakdown strength[23,24], negating the benefits of increased dielectric constant for energy storage[25,26]. Moreover, the incorporation of a high volume of high-K ceramic particles into polymer matrices not only escalates dielectric loss and diminishes overall efficiency but also engenders a proliferation of interfacial defects due to their limited compatibility[27,28]. These defects compromise the quality of the dielectric film, consequently undermining its reliability. Furthermore, the intricate fabrication process poses significant challenges to the industrial-scale application of ceramic-polymer composites. The preparation of all-organic composite dielectric films represents another prevalent approach. Typically, ferroelectric materials poly(vinylidene fluoride) (PVDF) and its copolymers such as poly(vinylidene fluoride-*co*-hexafluoropropylene) (P(VDF-HFP)), poly(vinylidene fluoride-trifluoroethylene-chlorofluoroethylene) (P(VDF-TrFE-CFE))[12,29,30], are often combined with linear polymers like poly(methyl methacrylate) PMMA, polyimide (PI), and poly(ether ether ketone) (PEEK). Ferroelectric materials possess a high dielectric constant, enhancing polarization capability. However, their low breakdown strength constrains the enhancement of energy storage density. Fortunately, the high breakdown strength and low loss characteristics of linear materials serve to ameliorate the susceptibility of ferroelectric materials to breakdown, averting premature polarization saturation. This synergistic interaction enhances energy storage performance and optimizes the charge/discharge efficiency. The excellent compatibility of polymers endows all-organic composite films with enhanced quality and preserves the esteemed attributes of polymer dielectrics, including their lightweight nature, ease of processing, and inherent flexibility. These attributes confer all-organic composite films with distinct advantages for large-scale manufacturing and practical application. Nevertheless, all-organic dielectrics still contend with the challenge of low discharged energy density. Proposed solutions include blending and multi-layer structural strategies, each with its limitations. The blending strategy struggles to achieve high-discharged energy density and charge/discharge efficiency simultaneously[31–34]. While the multi-layer strategy, though viable, demands an adequate layer count to attain optimal performance, which complicates the manufacturing process and falls short of meeting the requirements of industrial applications[35–38]. Therefore, the development of an all-organic composite dielectric material that integrates high-discharged energy density with excellent charge/discharge efficiency remains an urgent research priority.

Herein, we engineered an all-organic dielectric film with an exquisite nano-submicron structure. It features a nano-submicron PMMA surface layer and a P(VDF-HFP)@PMMA core-sheath intermediate layer, prepared using electrospinning technology and a hot-pressing process. The electrospinning technology has been demonstrated to have exceptional flexibility in material preparation and precise control over multiple parameters, thereby streamlining the preparation process and aligning well with the demands of industrialization[39]. The core-sheath configuration is strategically designed to harness the high polarizability of the P(VDF-HFP) core layer and the superior breakdown strength of the PMMA sheath layer. The abundance of ferroelectric/linear interfaces introduced by the core-sheath structure facilitates interface polarization and mitigates conduction loss through their barrier effect. This dual action enhances both the discharged energy density and the charge/discharge efficiency of dielectrics. Furthermore, the nano-submicron PMMA surface layer elevates the charge injection barrier at the electrode/dielectric interface[40], without compromising the overall dielectric constant. The significant reduction in space charge injection substantially improves the breakdown strength of the all-organic composite dielectric, while enabling it to maintain excellent charge/discharge efficiency under high electric fields. Ultimately, the 40%–420 nm PMMA-P(VDF-HFP)@PMMA film exhibited an impressive discharged energy density of 13.72 J/cm^3 at a high electric field of 740 kV/mm. Remarkably, it also achieved a high charge/discharge efficiency of 80%. The superior architectural design of the all-organic dielectric films has successfully achieved simultaneous enhancement in both discharged energy density and charge/discharge efficiency. This innovative structural design establishes a paradigm for the development of composite dielectric films that exhibit high breakdown strength, high efficiency, and substantial energy storage capabilities.

Results and discussion

Design strategies for the all-organic film

P(VDF-HFP), a ferroelectric copolymer of PVDF, is renowned for its exceptional polarization capacity, making it a preferred material in energy storage polymers. However, its low breakdown strength limits its range of applications. Conversely, as a linear polymer, PMMA's large bandgap confers advantages in restricting charge migration and enhancing breakdown strength. Figure 1 illustrates the fabrication process of an all-organic composite dielectric film via the process of coaxial electrospinning and hot-pressing. Initially, a series of core-sheath dielectric films with varying compositions of P(VDF-HFP)@PMMA were synthesized, to observe and select the sample exhibiting optimal dielectric performance under identical conditions. Transmission electron microscopy (TEM) has been employed to present the core-sheath structural fiber. In Fig. 1a$_1$, the sheath of PMMA (demarcated with orange lines) and the core of P(VDF-HFP) (indicated by white lines) are discernible, confirming the successful fabrication of the core-sheath structural fiber. According to the Poole–Frenkel effect, the large bandgap PMMA in the sheath layer, as the nano-submicron modification layer, can greatly limit electron migration and hopping conduction within P(VDF-HFP), thereby improving the breakdown strength and charge/discharge efficiency of the dielectric, as shown in Fig. 1a$_2$. Subsequently, the film was modified with a nano-submicron PMMA surface layer, resulting in an all-organic composite dielectric with structural features comprising a nano-submicron PMMA layer on the surface and a core-sheath structural film as the intermediate layer. The cross-sectional morphology of the composite structure film, modified with the nano-submicron PMMA surface layer and subjected to hot-pressing, was characterized using scanning electron microscopy (SEM) and is depicted in Fig. 1c$_1$. The nano-submicron PMMA surface layer is distinctly visible and the film exhibits uniformity and compactness. Under the Schottky effect, the high barrier at the electrode-dielectric interface effectively prevents electron injection from the electrode to the composite dielectric, especially under high electric fields, as shown in Fig. 1c$_2$. Therefore, the nano-submicron PMMA surface layer, as a secondary modification layer, effectively reduces excessive electron flow into the dielectric, thereby increasing the breakdown strength and improving charge/discharge efficiency through reduced conduction loss. All-organic films with nano-submicron PMMA surface layers of different thicknesses were prepared to assess their influence on the dielectric characteristics. The electrospinning process, during fabrication, exhibited remarkable flexibility and multi-parametric control, simplifying the process and facilitating the industrial scalability of high-discharged energy density polymer dielectrics.

Fabrication of the single core-sheath structural film

The compositional ratio of P(VDF-HFP)@PMMA is adjusted by modulating the flow rates of their precursor solutions, yielding a spectrum of core-sheath structural films with PMMA mass fractions of 30%, 40%, 45%, 50%, 60%, and 70%. To elucidate the dielectric characteristics of the composite, control specimens of pure P(VDF-

https://doi.org/10.1038/s41467-025-57249-z

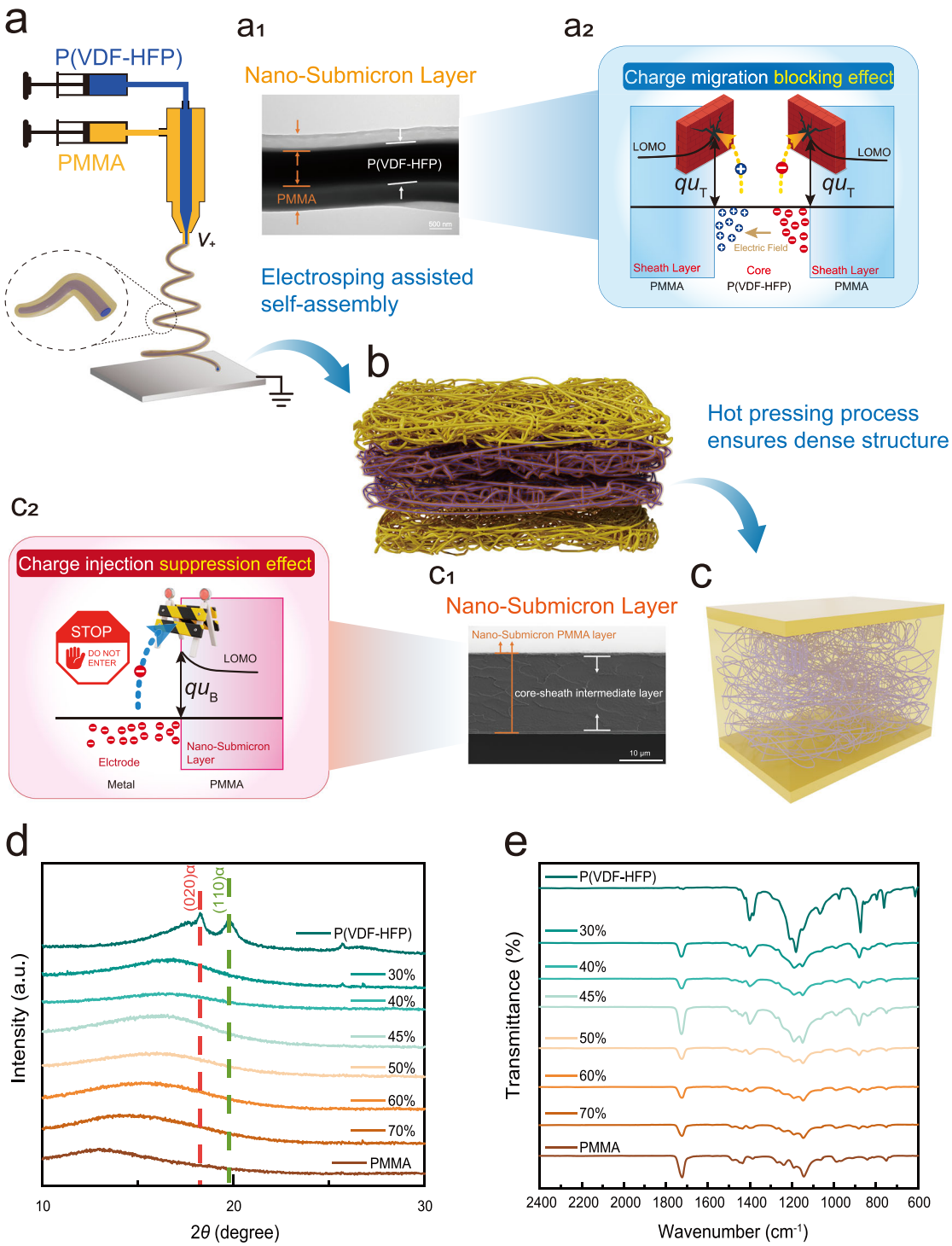

Fig. 1 | Schematic diagram of the preparation process and characterization of all-organic composite films. a–c Schematic diagram of the fabrication process of all-organic composite films via the process of coaxial electrospinning (**a**, **b**) and hot-pressing (**c**). **a$_1$** TEM image of the core-sheath structural fiber. **a$_2$** Schematic diagram of the nano-submicron layer suppressing the Poole–Frenkel effect. **c$_1$** SEM image of the cross-sectional morphology of the film with the nano-submicron surface layer. **c$_2$** Schematic diagram of the nano-submicron layer suppressing the Schottky effect. **d**, **e** XRD (**d**) patterns and FTIR (**e**) spectra of the single core-sheath structural films with different PMMA contents.

HFP) and PMMA films were crafted. The cross-sectional morphologies of the single core-sheath structural films obtained at different hot-pressing temperatures are summarized in Fig. S1, revealing that a continuous, uniform, and compact film is achievable at 180 °C.

Fabrication of the all-organic dielectric films with the nano-submicron surface layer

Selective electrospinning of PMMA was performed before and after the coaxial electrospinning process to fabricate composite structure films with a nano-submicron PMMA surface layer, while the precise

control of electrospinning duration for PMMA results in the formation of the PMMA surface layer with diverse thicknesses. A specialized difference of this process is where the P(VDF-HFP) precursor flow rate is zero and only the PMMA precursor flow rate is sustained while the hot-pressing process is the same as the core-sheath structural films. Figure S2 delineates the thicknesses of the nano-submicron PMMA surface layer resulting from 5, 10, 15, 20, and 25 min of electrospinning, corresponding to 190 nm, 240 nm, 380 nm, 420 nm, and 550 nm, respectively. Accordingly, the composite structure films with the nano-submicron PMMA surface layer were designated as 30%–190 nm, 30%–240 nm, 30%–380 nm, 30%–420 nm, 30%–550 nm, and the corresponding 40% components.

Characterization of all-organic composite films

Figure 1d presents the XRD patterns of the all-organic composite films. The distinct peaks at 18.3° and 19.9° can be attributed to the (020) and (110) planes of the α-phase in P(VDF-HFP)[41], whereas the PMMA exhibits an amorphous XRD pattern characterized by a broad hump at 13.02°[42]. Furthermore, the incorporation of PMMA results in the disappearance of the sharp peaks, replaced by a hump that shifts towards a lower angle with increasing PMMA content (towards the symmetry center of the PMMA hump). The FTIR spectra of the core-sheath structural films are displayed in Fig. 1e. Peaks at 763, 796, and 976 cm^{-1} in pure polymer P(VDF-HFP) are indicative of the α crystalline phase[43,44]. It is observed that the core-sheath structural films with varying PMMA mass fractions exhibit not only the characteristic peaks of P(VDF-HFP) but also those of PMMA, specifically at 1722 cm^{-1} (C=O) and 1200 cm^{-1} (C–O)[45]. XRD and FTIR analysis revealed consistent characteristics in the composite films with nano-submicron PMMA surface layers (as shown in Fig. S3).

Dielectric properties of P(VDF-HFP)@PMMA core-sheath structural films

In pursuit of the optimal compositional ratio, a series of core-sheath structural films with different P(VDF-HFP)@PMMA components were fabricated, alongside pure PMMA and P(VDF-HFP) films. This was conducted to scrutinize the evolution of the dielectric properties within the core-sheath structural films. Figure 2a delineates the dielectric constant and dielectric loss for the core-sheath structural films, as well as the pure PMMA and P(VDF-HFP) films, across a frequency spectrum from 1 Hz to 10 MHz. It is observed that the dielectric constant exhibits a gradual decline as the frequency ascends from 1 Hz to 10 MHz. As the mass fraction of PMMA escalates, the dielectric constant of the P(VDF-HFP)@PMMA films experiences a transition from a rapid to a gradual decline. This phenomenon is predominantly attributed to the shift in the matrix of the films from P(VDF-HFP) to PMMA. The dielectric constant of P(VDF-HFP) and core-sheath structural films decreases at frequencies above 100 kHz, which is attributed to α-relaxation caused by the polymer chain motion in the P(VDF-HFP) polymer matrix. Except for a minor increase in dielectric loss at low frequencies for the 30% PMMA samples, the dielectric loss across other samples was effectively mitigated. The incorporation of the linear polymer PMMA serves to suppress the overall dielectric loss of the film. Furthermore, the multitude of micro-interfaces between the linear and ferroelectric phases within the core-sheath configuration, limit the migration of charge carriers, further reducing the dielectric loss and enhancing the interfacial polarization. Notably, the dielectric loss of certain core-sheath structural films is observed to be lower than that of the linear PMMA material at low frequencies, underscoring the superior effectiveness of the core-sheath structure in reducing dielectric loss. When the frequency exceeds 100 kHz, the dielectric loss increases, primarily due to α-relaxation, and dipole relaxation within the P(VDF-HFP) matrix, and at the linear/ferroelectric interfaces. Additionally, the local electric field generated by the interaction between interfacial charges and the dipole field of P(VDF-HFP) further contributes to the increase in dielectric loss[46].

The relationship between the breakdown strength and energy storage performance is quadratic, emphasizing its significance for dielectrics with a high-discharged energy density. To assess the characteristic breakdown strength of all-organic films, the two-parameter Weibull statistical distribution is employed, mathematically expressed as $P(E) = 1\text{-}\exp[-(E/E_b)^{\beta}]$. Where $P(E)$ represents the cumulative probability of electrical failure, E denotes the experimental breakdown strength, E_b signifies the characteristic breakdown strength—where a 63.2% failure probability under this electric field and β is the shape parameter, indicative of the data dispersion[47]. The breakdown strength data for the core-sheath structural films are depicted in Fig. 2b. It is observed that an increase in PMMA content from 30% to 70% results in an enhancement of the breakdown strength from 443 kV/mm to 663 kV/mm of the films, which exceeds 55% of P(VDF-HFP) (426 kV/mm). This improvement is primarily attributed to the uniform confinement of P(VDF-HFP) in the large bandgap PMMA sheath, which suppresses the Poole–Frenkel effect[2] expressed as:

$$J_{PF} = \sigma_0 E \exp\left[\frac{-q(\mu_T - \sqrt{qE/\pi\varepsilon_0\varepsilon_r})}{k_B T}\right] \quad (1)$$

where σ_0 is the conductivity under a low electric field, q is the electronic charge, T is absolute temperature, k_B is Boltzmann's constant, and $q\mu_T$ is the barrier height of charge traps that is proportional to the bandgap of the corresponding material. The bandgap has been measured through the UV-vis absorption spectra[48] and the result shows that the bandgap of PMMA (3.22 eV) is significantly larger than that of PVDF-HFP (2.15 eV) as illustrated in Fig. S4. The introduction of numerous ferroelectric/linear micro-interfaces by the core-sheath structure significantly impedes carrier migration which improves the breakdown strength of the sheath-core structural films.

Figure 2c depicts the D–E curves (displacement–electric field) for the core-sheath structural films at an electric field of 300 kV/mm (Extracted from Fig. S5). The curve of P(VDF-HFP) demonstrates a pronounced breadth, indicating low charge/discharge efficiency and significant energy loss during the processes of polarization and depolarization. With the incorporation of PMMA into the sheath and an increase in its content, the D–E curve progressively narrows, indicating an enhancement in the charge/discharge efficiency of the core-sheath structural films. This enhancement can be primarily attributed to two key factors. First, the PMMA sheath suppresses the aggregation of ferroelectric phase P(VDF-HFP), forming numerous linear/ferroelectric interfaces that effectively impede carrier migration through the Poole–Frenkel effect, thereby reducing conduction losses[46]. Second, the introduction of the linear material PMMA also plays a positive role in reducing the energy loss of the film. The remanent polarization (P_r), charge/discharge efficiency, and discharged energy density of the samples are collected in Fig. 2d. It is observed that the P_r of the core-sheath structural films exhibits a significant decrease relative to pure P(VDF-HFP) sample, and the increased content of the linear polymer PMMA leads to a further reduction in P_r, even though with a more moderate trend. With the restriction of the P_r, the film's charge/discharge efficiency is enhanced from 63% (for pure P(VDF-HFP)) to 89% (for the 70% core-sheath structural film). Once the PMMA content exceeds 40%, the charge/discharge efficiency stabilizes at a level above 80%. The findings align with the D–E curve data of the core-sheath structural films (Fig. 2c). The merits of the core-sheath structure are further exemplified in Fig. S6, where a comparative analysis of the 40% core-sheath structural film fabricated in this work and the films with the same PMMA content, prepared using the blending method, reveals that the dielectric constant and breakdown strength of the former

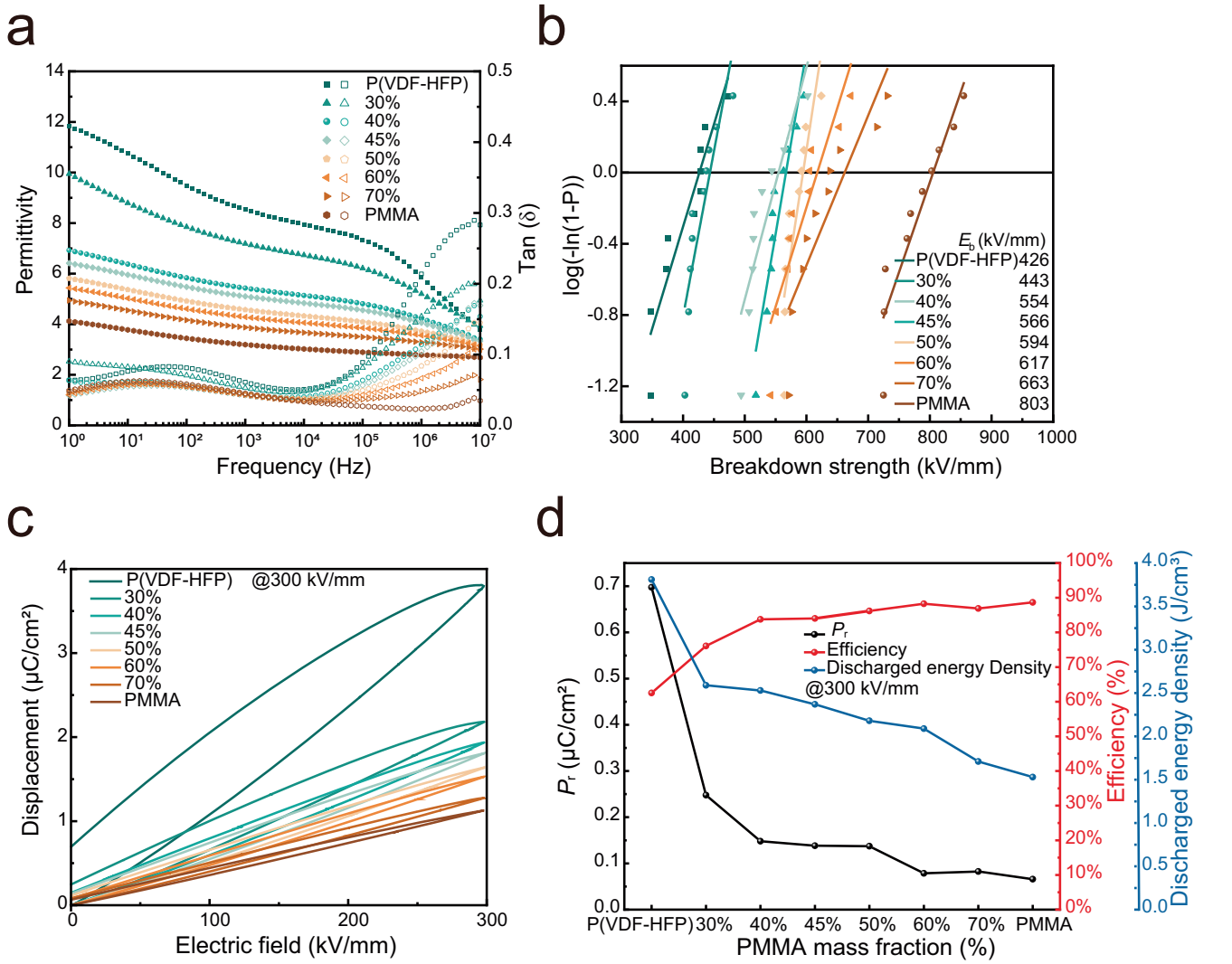

Fig. 2 | Dielectric properties of P(VDF-HFP), PMMA, and core-sheath structural films. a–c Dielectric constant and dielectric loss (**a**), breakdown strength (**b**), and *D*–*E* curves (**c**) of the films. **d** P_r, charge/discharge efficiency, and discharged energy density of the films at 300 kV/mm.

surpasses those of the latter while maintaining the equivalent dielectric loss. A representative finite element method has demonstrated that the fibrous morphology is more conducive to improving the dielectric constant by rationally allocating the local electric field distribution, as illustrated in Fig. S7. This simultaneous enhancement of both dielectric constant and breakdown strength at a given mass fraction addresses the inherent conflict between the two parameters. It is attributed to the core-sheath structural film fabricated via electrospinning technology ensuring uniform dispersion of P(VDF-HFP) within the PMMA matrix. Figure S8 presents a trend chart for the dielectric constant and breakdown strength of the core-sheath structural films with varying PMMA compositions. Given that discharged energy density depends on both the dielectric constant and breakdown strength, a nano-submicron PMMA surface layer is designed for the 30% and 40% core-sheath structural films to further enhance the energy storage capabilities of the dielectrics.

Dielectric and energy storage properties of nano-submicron surface layer PMMA-P(VDF-HFP)@PMMA composites

To further enhance the energy storage capabilities of the core-sheath structural films, a series of nano-submicron surface layer PMMA-P(VDF-HFP)@PMMA composite films, with varying surface PMMA layer thicknesses, were fabricated and analyzed for their impact on the dielectric characteristics. The surface PMMA layer thickness for all samples was precisely controlled at the nano-submicron scale. Figure 3a illustrates the variation in dielectric constant and loss for nano-submicron surface layer films with 30% and 40% of PMMA content in core-sheath structural at 1 kHz (Extracted from Fig. S9). The dielectric constant decreases by 31% and 17% for the 30% and 40% samples, respectively, as the surface PMMA layer becomes thicker. This is primarily due to the inherent low dielectric constant of PMMA. The dielectric loss of the all-organic composite films remains consistently low. Figure 3b displays the breakdown strength (Weibull distribution of the breakdown strength is shown in Fig. S10) and the charge/discharge efficiency at 500 kV/mm of the nano-submicron surface layer films. The nano-submicron surface layer films exhibit a higher breakdown strength, with improvements of 38% and 16% compared to the 30% and 40% core-sheath structural films, respectively. This improvement can be primarily attributed to two factors. First, the large bandgap nano-submicron PMMA surface layer effectively suppresses Schottky injection of charges[2], as below:

$$J_S = AT^2 \exp\left[\frac{-q(\mu_B - \sqrt{qE/4\pi\varepsilon_0\varepsilon_r})}{k_B T}\right] \quad (2)$$

https://doi.org/10.1038/s41467-025-57249-z

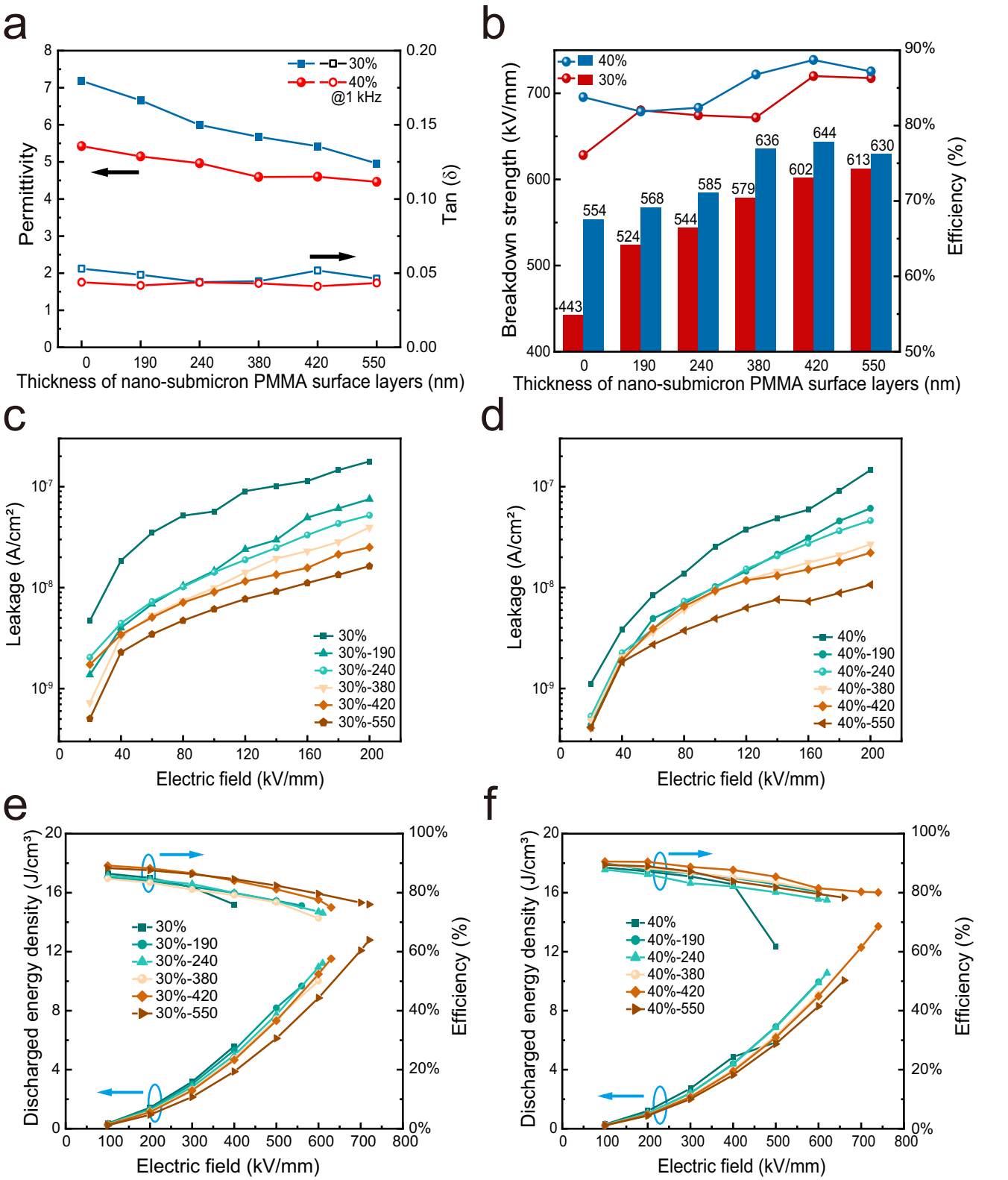

Fig. 3 | Dielectric properties of the nano-submicron surface layer films with different thicknesses of the PMMA layer. a Dielectric constant and dielectric loss of 30% and 40% nano-submicron surface layer films. **b** Breakdown strength and charge/discharge efficiency of 30% and 40% nano-submicron surface layer films. **c**, **d** Leakage current density of 30% (**c**) and 40% (**d**) nano-submicron surface layer films. **e**, **f** Discharged energy density and charge/discharge efficiency of 30% (**e**) and 40% (**f**) nano-submicron surface layer films.

where A is the Richardson constant, T is absolute temperature, q is the electronic charge, k_B is Boltzmann's constant, and $q\mu_B$ is the barrier height. Therefore, the larger bandgap of PMMA is more effective in reducing space charge injection and mitigating its adverse effects on breakdown performance[41]. Second, the internal coaxial structure suppresses the aggregation of the ferroelectric phase, while the large bandgap PMMA sheath hinders the charge transport, thereby limiting the development of the breakdown electrical tree. The nano-

https://doi.org/10.1038/s41467-025-57249-z

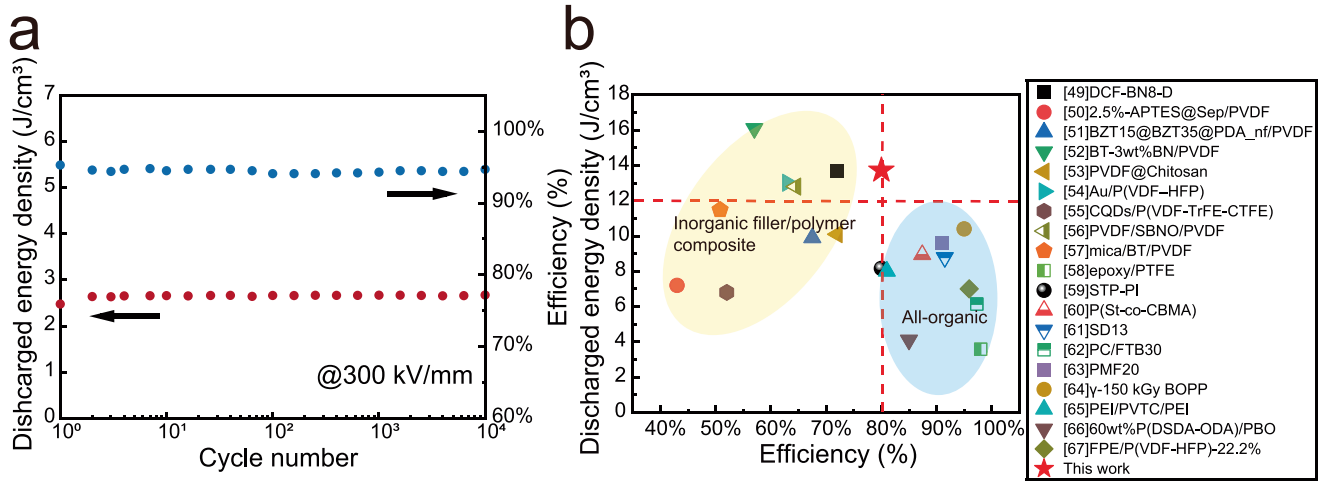

Fig. 4 | Reliability and energy storage performance of the 40%–420 nm PMMA-P(VDF-HFP)@PMMA film. a Charge/discharge cycle performance at 300 kV/mm. **b** Comparison of the discharged energy density and charge/discharge efficiency between this work and recent reports.

submicron surface layer films of 40% surpass the 30% samples in breakdown strength, due to the higher PMMA component. When the thickness of the PMMA surface layer in the 40% samples reaches 380 nm, further increases do not yield additional improvements in breakdown strength, suggesting an approach to the intrinsic limit of the intermediate core-sheath structure layer. Moreover, the nano-submicron surface layer films generally demonstrate an improved charge/discharge efficiency, which increases with the thickness of the nano-submicron PMMA surface layer, corroborated by the thinning *D*–*E* curve in Figs. S11 and S12 as the PMMA surface layer thickness increases. Since there is a quadratic relationship between breakdown strength and discharged energy density, a strategic reduction in dielectric constant to achieve a proportional enhancement in breakdown strength is advantageous. This approach not only enhances energy storage performance but also elevates charge/discharge efficiency, affirming the efficacy of the nano-submicron surface layer design.

The influence of the nano-submicron surface layer on the breakdown strength and charge/discharge efficiency was elucidated through an examination of the conductive performance under low field conditions. As depicted in Fig. 3c, d the nano-submicron surface layer films exhibit a significantly enhanced suppression of leakage current density compared to the core-sheath structural films, with a reduction of one order of magnitude under equivalent field strengths. Notably, the leakage current density of the nano-submicron surface layer films diminishes further with increasing PMMA surface layer thickness. For instance, at 200 kV/mm, the leakage current densities for the 30% and 40% core-sheath structural films are 1.77×10^{-7} A/cm² and 1.46×10^{-7} A/cm², respectively, whereas the corresponding densities of the nano-submicron surface layer films achieve 1.63×10^{-8} A/cm² and 1.06×10^{-8} A/cm². This substantial reduction in leakage current density contributes to the suppression of the space charge injection by the large bandgap nano-submicron PMMA surface layer. Therefore, the nano-submicron surface layer films exhibit superior breakdown strength and charge/discharge efficiency. The discharged energy density and charge/discharge efficiency of the nano-submicron surface layer films and the core-sheath structural films are compared, as shown in Fig. 3e, f (Extracted from Fig. S13). The nano-submicron surface layer films confer superior breakdown strength, enabling higher polarization at elevated field strengths and considerably surpassing the core-sheath structural films in discharged energy density. Moreover, the nano-submicron surface layer films are characterized by a higher charge/discharge efficiency, with the 40% samples showcasing exceptional stability across all field strengths. This enhancement mainly comes from the reduced space charge injection and conduction loss caused by the nano-submicron PMMA surface layer, confirming the results of the leakage current density analysis. At identical field strengths, the 30% nano-submicron surface layer films exhibited superior discharged energy density, attributed to the enhanced polarization capability from its high P(VDF-HFP) content. Correspondingly, the 40% nano-submicron surface layer films showed a higher charge/discharge efficiency. Finally, the 40%–420 nm PMMA-P(VDF-HFP)@PMMA film achieved an exceptional combination of a high charge/discharge efficiency of 80% and a substantial discharged energy density of 13.72 J/cm³ under a high electric field of 740 kV/mm. The discharged energy density and charge/discharge efficiency achieved a respective increase of 137% and 32% compared to P(VDF-HFP) (Fig. S14). To verify the universality of the proposed nano-submicron structure, we selected two common linear polymers, polycarbonate (PC) and polystyrene (PS), to replace PMMA. Core-sheath structural films and nano-submicron surface layer films based on PC and PS were prepared, and their dielectric properties are shown in Figs. S15–S19, which exhibit consistent patterns of variation, including enhanced breakdown field strength, reduced dielectric loss, and decreased leakage current density. As a result, the discharged energy density and charge/discharge efficiency of the PC-based nano-submicron surface layer film (NSSL-PC-40%) are 5.99 J/cm³ and 82% at 600 kV/mm, respectively, both surpassing those of P(VDF-HFP). The discharged energy density and charge/discharge efficiency of the PS-based nano-submicron surface layer film (NSSL-PS-50%) are 4.42 J/cm³ and 84% at 500 kV/mm, with the former comparable to P(VDF-HFP) and the latter significantly higher. To summarize, by virtue of its structural and barrier advantages, the nano-submicron structure is effective in synergistically improving the discharged energy density and charge/discharge efficiency.

A cyclic charge/discharge test was performed to examine the long-term reliability of the 40%–420 nm PMMA-P(VDF-HFP)@PMMA film. As shown in Fig. 4a, the 40%–420 nm PMMA-P(VDF-HFP)@PMMA film exhibits stable discharged energy density and charge/discharge efficiency (over 90%) after 1×10^4 cycles at 300 kV/mm. Figure 4b is a summary of the discharged energy density and charge/discharge efficiency of organic/inorganic composite and all-organic composite dielectrics in recent years[49–67]. The key dielectric parameters are summarized in Table S1 in the Supporting Information. Although the maximum discharged energy density of the reported composite dielectrics is excellent, their charge/discharge efficiency is still unsatisfactory. Surprisingly, the nano-submicron surface layer films

prepared in this work possess both excellent discharged energy density and superior charge/discharge efficiency. It merits emphasis although the addition of inorganic fillers increases the discharged energy density of the composite dielectric materials, this increase is at the expense of increasing the interface defects between the matrix and the particles, which will greatly damage the mechanical properties of the polymer matrix. These factors introduce significant challenges to the industrial-scale production of composite dielectric films, rendering mass manufacturing a formidable endeavor. Thus, the all-organic dielectric film with the nano-submicron surface layer holds considerable significance for achieving substantial discharged energy density with a high charge/discharge efficiency. This accomplishment is primarily attributed to the superior structural design, which endows the film with both high-component ferroelectric materials and excellent breakdown strength that are typically mutually exclusive.

This work proposes an all-organic dielectric film with a nano-submicron surface layer, aiming to address the limitations of P(VDF-HFP)-based polymers for energy storage applications. The core-sheath structure disperses P(VDF-HFP) within PMMA, preventing the aggregation of the ferroelectric phase. The introduced numerous ferroelectric/linear micro-interfaces hinder the migration of charge carriers, significantly improve the breakdown strength, and promote interfacial polarization, resulting in a simultaneous increase in the dielectric constant and breakdown strength. In addition, the nano-submicron PMMA surface layer improves the charge injection barrier at the dielectric/electrode interface, mitigates the effect of space charge on the breakdown strength, and limits the dielectric conduction loss by limiting space charge injection. At an electric field of 740 kV/mm, the film achieves a high charge/discharge efficiency of 80% and a respectable discharged energy density of 13.72 J/cm^3, providing a promising approach for the development of efficient, economical, and industrially scalable energy storage dielectrics.

Methods

Materials

P(VDF-HFP) particles were purchased from PolyK Technologies. PMMA particles and N, N-dimethylformamide were purchased from Shanghai Aladdin Biochemical Technology Co., Ltd. Ethyl alcohol and deionized water were obtained from Tansoole (Beijing, China). Acetone was obtained from Beijing Tong Guang Fine Chemicals Company and all chemicals were used as received without further purification.

Preparation of the all-organic composite films

Core-sheath structural films: In this work, the core-sheath structural film was fabricated by coaxial spinning technology and hot-pressing. Specifically, P(VDF-HFP) particles were dissolved in a mixed solvent of DMF and acetone (3:2 volume ratio) to get a 0.15 g/mL solution as the core layer precursor (solution A), PMMA particles were dissolved in a mixed solvent of DMF and acetone (3:2 volume ratio) to get a 0.2 g/mL solution as the sheath layer precursor (solution B). The two kinds of precursors were stirred for 8 h at 50 °C. The solutions A and B were then placed into coaxially connected syringes, and electrospun with an electric field of 1 kV cm^{-1}. The mass ratio of P(VDF-HFP)@PMMA was controlled by controlling the core-sheath injection ratio. The electrospinning time of all the core-sheath structural films was 2 h. The as-spun fibrous mats were hot-pressed at 180 °C for 30 min under a pressure of 8 MPa and then the as-pressed films were quenched under cold pressing at 25 °C for 10 min followed by drying at 80 °C for 12 h.

All-organic films with nano-submicron PMMA surface layers: a layer of PMMA is first electrospun on the collector, then the core-sheath fiber is electrospun, and finally the outermost layer of PMMA is electrospun. The entire process is accomplished by adjusting the syringe. Besides, different thicknesses of the nano-submicron surface layer were prepared with different electrospinning times of the PMMA. In this work, we prepared pure P(VDF-HFP) and PMMA samples, as well as P(VDF-HFP)@PMMA core-sheath structural films with PMMA mass fractions of 30%, 40%, 45%, 50%, 60%, and 70%. On the basis of the core-sheath structural films, nano-submicron surface layer films 30%–190 nm, 30%–240 nm, 30%–380 nm, 30%–420 nm, 30%–550 nm, and 40%–190 nm, 40%–240 nm, 40%–380 nm, 40%–420 nm, 40%–550 nm were further prepared.

Characterizations

The cross-section of the nano-submicron surface layer films and the fiber morphology of the core-sheath structural films were characterized by TEM (Tecnai Spirit, FEI, USA) and SEM (JEOL JSM 6301 F, Japan). X-ray diffraction (D/max-2550, Rigaku, Japan) and Fourier transform infrared spectroscopy (X70, NETZSCH, Germany) were conducted to study the crystal structure of all-organic films using Cu Kα source. Dielectric properties of the all-organic composite films were measured by a Broadband Dielectric Spectroscopy (Novocontrol Technologies GmbH & Co. KG, Germany) in the frequency range from 10^0 to 10^7 Hz. The breakdown of the all-organic composite films was conducted on the Dielectric Withstand Voltage Test System (Beiguang Jingyi Instrument Equipment Co., Ltd, China). Unipolar displacement–electric field (D–E) hysteresis loops (at 10 Hz) were carried out with a Premier II ferroelectric test system (Radiant Technologies Inc, USA). The leakage current was measured by a combination of the power supply (Keithley, 2290-10, USA) and System SourceMeter (Keithley, 2635B, USA).

Data availability

The authors declare that all data supporting the findings of this study are available within the article and the supplementary materials. Further information is available from the corresponding author upon request (dangzm@tsinghua.edu.cn).

References

1. Chu, B. et al. A dielectric polymer with high electric energy density and fast discharge speed. *Science* **313**, 334–336 (2006).
2. Feng, Q.-K. et al. Recent progress and future prospects on all-organic polymer dielectrics for energy storage capacitors. *Chem. Rev.* **122**, 3820–3878 (2022).
3. Yang, M. Z. et al. Roll-to-roll fabricated polymer composites filled with subnanosheets exhibiting high energy density and cyclic stability at 200 °C. *Nat. Energy* **9**, 14 (2024).
4. Wang, R. et al. Designing tailored combinations of structural units in polymer dielectrics for high-temperature capacitive energy storage. *Nat. Commun.* **14**, 11 (2023).
5. Kim, J. et al. Ultrahigh capacitive energy density in ion-bombarded relaxor ferroelectric films. *Science* **369**, 81–84 (2020).
6. Wang, L. W., Huang, X. Y., Zhu, Y. K. & Jiang, P. K. Enhancing electrical energy storage capability of dielectric polymer nanocomposites via the room temperature Coulomb blockade effect of ultrasmall platinum nanoparticles. *Phys. Chem. Chem. Phys.* **20**, 5001–5011 (2018).
7. Liu, F. H. et al. High-energy-density dielectric polymer nanocomposites with trilayered architecture. *Adv. Funct. Mater.* **27**, 7 (2017).
8. Zheng, M. S. et al. Improved dielectric, tensile and energy storage properties of surface rubberized $BaTiO_3$/polypropylene nanocomposites. *Nano Energy* **48**, 144–151 (2018).
9. Li, L. et al. Significant improvements in dielectric constant and energy density of ferroelectric polymer nanocomposites enabled by ultralow contents of nanofillers. *Adv. Mater.* **33**, 9 (2021).
10. Ai, D. et al. Tuning nanofillers in in situ prepared polyimide nanocomposites for high-temperature capacitive energy storage. *Adv. Energy Mater.* **10**, 7 (2020).

11. Zhu, Y. K. et al. High energy density polymer dielectrics interlayered by assembled boron nitride nanosheets. *Adv. Energy Mater.* **9**, 1 (2019).
12. Prateek, Thakur, V. K. & Gupta, R. K. Recent progress on ferroelectric polymer-based nanocomposites for high energy density capacitors: synthesis, dielectric properties, and future aspects. *Chem. Rev.* **116**, 4260–4317 (2016).
13. Chi, Q. G. et al. Significantly enhanced energy storage density for poly(vinylidene fluoride) composites by induced PDA-coated $0.5Ba(Zr_{0.2}Ti_{0.8})O_3$-$0.5(Ba_{0.7}Ca_{0.3})TiO_3$ nanofibers. *J. Mater. Chem. A* **5**, 16757–16766 (2017).
14. Shen, Z. H. et al. Phase-field model of electrothermal breakdown in flexible high-temperature nanocomposites under extreme conditions. *Adv. Energy Mater.* **8**, 8 (2018).
15. Jaidka, S. & Singh, D. P. Ultrahigh efficiency and enhanced discharge energy density at low loading of nanofiller in trilayered polyvinylidene fluoride-$Ba_{0.8}Sr_{0.2}TiO_3$ nanocomposites. *Polym. Compos.* **45**, 4561–4572 (2024).
16. Huang, X. Y., Sun, B., Zhu, Y. K., Li, S. T. & Jiang, P. K. High-k polymer nanocomposites with 1D filler for dielectric and energy storage applications. *Prog. Mater. Sci.* **100**, 187–225 (2019).
17. Pan, Z. B., Yao, L. M., Zhai, J. W., Yao, X. & Chen, H. Interfacial coupling effect in organic/inorganic nanocomposites with high energy density. *Adv. Mater.* **30**, 7 (2018).
18. Zhang, X. et al. Giant energy density and improved discharge efficiency of solution-processed polymer nanocomposites for dielectric energy storage. *Adv. Mater.* **28**, 2055–2061 (2016).
19. Luo, B. C. et al. Superhierarchical inorganic/organic nanocomposites exhibiting simultaneous ultrahigh dielectric energy density and high efficiency. *Adv. Funct. Mater.* **31**, 11 (2021).
20. Hu, H. L. et al. Recent advances in rational design of polymer nanocomposite dielectrics for energy storage. *Nano Energy* **74**, 20 (2020).
21. Wu, D., Zhai, Y., Xu, H. & Guo, L. Synergistic enhancement of dielectric properties of polymer matrix composites by micro-nano bicomponent ceramics and conductive particles. *IET Nanodielectr.* **6**, 1–8 (2023).
22. Zhang, N. et al. Improved energy storage property in polyvinylidene fluoride-based multilayered composite regulated by oriented carbon nanotube@SiO_2 nanowires. *IET Nanodielectr.* **6**, 19–31 (2023).
23. Zhang, T. et al. An alternating multilayer architecture boosts ultrahigh energy density and high discharge efficiency in polymer composites. *RSC Adv.* **10**, 5886–5893 (2020).
24. Luo, S. B. et al. Significantly enhanced electrostatic energy storage performance of flexible polymer composites by introducing highly insulating-ferroelectric microhybrids as fillers. *Adv. Energy Mater.* **9**, 7 (2019).
25. Luo, H. et al. Improved dielectric properties and energy storage density of poly(vinylidene fluoride-co-hexafluoropropylene) nanocomposite with hydantoin epoxy resin coated $BaTiO_3$. *ACS Appl. Mater. Interfaces* **7**, 8061–8069 (2015).
26. Li, Q., Han, K., Gadinski, M. R., Zhang, G. Z. & Wang, Q. High energy and power density capacitors from solution-processed ternary ferroelectric polymer nanocomposites. *Adv. Mater.* **26**, 6244–6249 (2014).
27. Li, H. et al. Ternary polymer nanocomposites with concurrently enhanced dielectric constant and breakdown strength for high-temperature electrostatic capacitors. *InfoMat* **2**, 389–400 (2020).
28. Li, Q. et al. Solution-processed ferroelectric terpolymer nanocomposites with high breakdown strength and energy density utilizing boron nitride nanosheets. *Energy Environ. Sci.* **8**, 922–931 (2015).
29. Li, H. et al. Nanostructured ferroelectric-polymer composites for capacitive energy storage. *Small Methods* **2**, 18 (2018).
30. Zhang, Y. et al. Energy storage enhancement of P(VDF-TrFE-CFE)-based composites with double-shell structured BZCT nanofibers of parallel and orthogonal configurations. *Nano Energy* **66**, 13 (2019).
31. Zheng, M. S. et al. Enhanced breakdown strength of poly(vinylidene fluoride) utilizing rubber nanoparticles for energy storage application. *Appl. Phys. Lett.* **109**, 5 (2016).
32. Zheng, M. S. et al. Polyurethane induced high breakdown strength and high energy storage density in polyurethane/poly(vinylidene fluoride) composite films. *Appl. Phys. Lett.* **110**, 4 (2017).
33. Liu, F. H., Li, Z. Y., Wang, Q. & Xiong, C. X. High breakdown strength and low loss binary polymer blends of poly(vinylidene fluoride-trifluoroethylene-chlorofluoroethylene) and poly(methyl methacrylate). *Polym. Adv. Technol.* **29**, 1271–1277 (2018).
34. Xia, W. M., Zhang, Q. P., Wang, X. & Zhang, Z. C. Electrical energy discharging performance of poly(vinylidene fluoride-co-trifluoroethylene) by tuning its ferroelectric relaxation with polymethyl methacrylate. *J. Appl. Polym. Sci.* **131**, 9 (2014).
35. Lin, X. et al. Enhanced dielectric properties of immiscible poly (vinylidene fluoride)/low density polyethylene blends by inducing multilayered and orientated structures. *Compos. Part B Eng.* **114**, 58–68 (2017).
36. Mackey, M. et al. Reduction of dielectric hysteresis in multi layered films via nanoconfinement. *Macromolecules* **45**, 1954–1962 (2012).
37. Carr, J. M. et al. Effect of biaxial orientation on dielectric and breakdown properties of poly(ethylene terephthalate)/poly(-vinylidene fluoride-co-tetrafluoroethylene) multilayer films. *J. Polym. Sci. Part B Polym. Phys.* **51**, 882–896 (2013).
38. Zhou, Z. et al. Interphase/interface modification on the dielectric properties of polycarbonate/poly(vinylidene fluoride-co-hexafluoropropylene) multilayer films for high-energy density capacitors. *J. Polym. Sci. Part B Polym. Phys.* **51**, 978–991 (2013).
39. Ji, D. et al. Electrospinning of nanofibres. *Nat. Rev. Methods Prim.* **4**, 1 (2024).
40. Zhou, Y. et al. A scalable, high-throughput, and environmentally benign approach to polymer dielectrics exhibiting significantly improved capacitive performance at high temperatures. *Adv. Mater.* **30**, 7 (2018).
41. Jiang, J. Y. et al. Polymer nanocomposites with interpenetrating gradient structure exhibiting ultrahigh discharge efficiency and energy density. *Adv. Energy Mater.* **9**, 9 (2019).
42. Vuluga, Z. et al. Morphological and tribological properties of PMMA/halloysite nanocomposites. *Polymers* **10**, 23 (2018).
43. Jiang, J. Y. et al. Tuning phase composition of polymer nanocomposites toward high energy density and high discharge efficiency by nonequilibrium processing. *ACS Appl. Mater. Interfaces* **9**, 29717–29731 (2017).
44. Shenbagavalli, S., Muthuvinayagam, M. & Revathy, M. S. Electrical properties of Mg^{2+} ion-conducting PEO: P(VdF-HFP) based solid blend polymer electrolytes. *Polymer* **256**, 15 (2022).
45. Jiang, S. H. et al. Preparation of functionalized graphene by simultaneous reduction and surface modification and its polymethyl methacrylate composites through latex technology and melt blending. *Chem. Eng. J.* **226**, 326–335 (2013).
46. Jaidka, S. & Singh, D. P. Tailored multilayered films of the PVDF/$Ba_{0.8}Sr_{0.2}TiO_3$ nanocomposites with surface-modified nanoparticles for superior dielectric and energy storage performance. *J. Alloy Compd.* **1003**, 10 (2024).
47. Han, K. et al. A hybrid material approach toward solution-processable dielectrics exhibiting enhanced breakdown strength and high energy density. *Adv. Funct. Mater.* **25**, 3505–3513 (2015).
48. Jasuja, K. et al. Introduction of protonated sites on exfoliated, large-area sheets of hexagonal boron nitride. *ACS Nano* **12**, 9931–9939 (2018).

49. Tu, H. et al. High strength and biodegradable dielectric film with synergistic alignment of chitosan nanofibrous networks and BNNSs. *Carbohydr. Polym.* **299**, 10 (2023).
50. Chen, S. N. et al. Polymer-based dielectric nanocomposites with high energy density via using natural sepiolite nanofibers. *Chem. Eng. J.* **401**, 13 (2020).
51. Hu, J., Liu, Y., Zhang, S. F. & Tang, B. T. Novel designed core-shell nanofibers constituted by single element-doped $BaTiO_3$ for high-energy-density polymer nanocomposites. *Chem. Eng. J.* **428**, 9 (2022).
52. Guo, R. et al. Bilayer structured PVDF-based composites via integrating $BaTiO_3$ nanowire arrays and BN nanosheets for high energy density capacitors. *Chem. Eng. J.* **437**, 11 (2022).
53. Che, J. J. et al. High-energy-density waterborne dielectrics from polyelectrolyte-colloid complexes. *Adv. Funct. Mater.* **33**, 9 (2023).
54. Xia, S. M. et al. Achieving remarkable energy storage enhancement in polymer dielectrics via constructing an ultrathin Coulomb blockade layer of gold nanoparticles. *Mater. Horiz.* **10**, 2476–2486 (2023).
55. Jiang, X. et al. Ultralow loading of carbon quantum dots leading to significantly improved breakdown strength and energy density of P(VDF-TrFE-CTFE). *J. Mater. Chem. A* **11**, 16127–16137 (2023).
56. Ryu, A. et al. Layer-controlled perovskite 2D nanosheet interlayer for the energy storage performance of nanocomposites. *Small* **19**, 8 (2023).
57. Ren, Y. J. et al. Significantly enhanced the energy density of dielectric composites by sandwich structure with highly insulating mica nanosheets. *Small* **20**, 9 (2024).
58. Luo, S. B. et al. Enhancement of dielectric breakdown strength and energy storage of all-polymer films by surface flattening. *Chem. Eng. J.* **412**, 8 (2021).
59. Zheng, W. W. et al. Temperature resistant amorphous polyimides with high intrinsic permittivity for electronic applications. *Chem. Eng. J.* **436**, 8 (2022).
60. He, G. H. et al. All-organic polymer dielectrics prepared via optimization of sequential structure of polystyrene-based copolymers. *Chem. Eng. J.* **446**, 11 (2022).
61. Liang, Y. J. et al. Sulfonyl manipulation for enhancing energy storage of flexible epoxy based capacitive films. *Chem. Eng. J.* **484**, 10 (2024).
62. Li, T. Y. et al. Constructing fluorinated triphenyl in carbonate copolymers toward flexible high energy-storable dielectric films with enhanced thermal resistance. *Nano Energy* **130**, 15 (2024).
63. Li, D. L. et al. Scalable in-situ microfibrillar dielectric films: achieving exceptional energy density and efficiency. *Energy Storage Mater.* **72**, 10 (2024).
64. Wang, Y. W. et al. γ-ray irradiation significantly enhances capacitive energy storage performance of polymer dielectric films. *Adv. Mater.* **36**, 2308597 (2024).
65. Wang, C. et al. Enhanced performance of all-organic sandwich structured dielectrics with linear dielectric and ferroelectric polymers. *J. Mater. Chem. A* **9**, 8674–8684 (2021).
66. Zuo, P. Y. et al. Scalable co-cured polyimide/poly(p-phenylene benzobisoxazole) all-organic composites enabling improved energy storage density, low leakage current and long-term cycling stability. *Mater. Horiz.* **11**, 271–282 (2024).
67. Liu, S. Y. et al. The simple synthesis of all-organic polymer bilayer films: achieving simultaneous enhancements in energy storage density and efficiency. *J. Appl. Polym. Sci.* **140**, 9 (2023).

Acknowledgements

This work was financially supported by the National Key Research and Development Program of China (Grants No. 2021YFA0718801 to Y.N.H. and No. 2021YFB2401502 to Z.M.D.), the National Natural Science Foundation of China (Grants No. 52107018 to S.L.Z., No. U2241243 to K.B., and No. 52437002 to Z.M.D.), and the Beijing Natural Science Foundation (Grant No. JQ22010 to K.B.).

Author contributions

Z.M.D., S.L.Z., and K.X. conceived the idea; K.X., Z.M.D., and S.L.Z. designed the experiments; K.X. and S.L.Z. carried out most of the experiment work; X.J.W., L.H., Y.G., T.L., and Y.M. helped with the high-field dielectric measurements; K.X., Z.M.D., K.B., S.L.Z., Y.N.H., X.J.W., and L.H. analyzed the data. K.X., Z.M.D., K.B., and S.L.Z. wrote the manuscript and all authors participated in manuscript revision.

Competing interests

The authors declare no competing interests.

Additional information

Supplementary information The online version contains supplementary material available at https://doi.org/10.1038/s41467-025-57249-z.

Correspondence and requests for materials should be addressed to Ke Bi, Shao-Long Zhong or Zhi-Min Dang.

Peer review information *Nature Communications* thanks Dwijendra P. Singh, and the other, anonymous, reviewer(s) for their contribution to the peer review of this work. A peer review file is available.